

## MIT Open Access Articles

*Quantum nonlinear optics using cold Rydberg atoms*

The MIT Faculty has made this article openly available. **Please share** how this access benefits you. Your story matters.

**Citation:** Peyronel, T., O. Firstenberg, Q.-Y. Liang, A. Gorshkov, M. D. Lukin, and V. Vuletic. "Quantum Nonlinear Optics Using Cold Rydberg Atoms." Edited by Zameer U. Hasan, Philip R. Hemmer, Hwang Lee, and Charles M. Santori. *Advances in Photonics of Quantum Computing, Memory, and Communication VII* (February 19, 2014). © 2014 Society of Photo-Optical Instrumentation Engineers (SPIE)

**As Published:** <http://dx.doi.org/10.1117/12.2043165>

**Publisher:** SPIE

**Persistent URL:** <http://hdl.handle.net/1721.1/98462>

**Version:** Final published version: final published article, as it appeared in a journal, conference proceedings, or other formally published context

**Terms of Use:** Article is made available in accordance with the publisher's policy and may be subject to US copyright law. Please refer to the publisher's site for terms of use.



# Quantum nonlinear optics using cold Rydberg atoms.

T. Peyronel<sup>a</sup>, O. Firstenberg<sup>b</sup>, Q.-Y. Liang<sup>a</sup>, A. Gorshkov<sup>c</sup>, M. D. Lukin<sup>b</sup>, V. Vuletic<sup>a</sup>

<sup>a</sup>Physics Department and Research Laboratory of Electronics, MIT, Cambridge, MA, USA;

<sup>b</sup>Physics Department, Harvard University, Cambridge, MA, USA;

<sup>c</sup>Joint Quantum Institute, NIST/University of Maryland, College Park, Maryland 20742, USA.

## ABSTRACT

Although photons do not affect each other in vacuum, interactions between individual photons could enable a wide variety of scientific and engineering applications. Here we report on the creation of a quantum nonlinear medium with large photon-photon interactions at the single photon level. Our approach relies on Electromagnetically Induced Transparency (EIT) techniques, in which individual photons are coherently mapped onto strongly interacting Rydberg atoms. Under EIT conditions, photons traveling in the medium are best described as part-matter part-light quantum particles, called polaritons, which experience long-range interactions through the Rydberg blockade. In particular, we demonstrate coherent photon-photon interactions, akin to those associated with conventional massive particles, paving the way for novel photonics states and quantum simulation with light.

**Keywords:** Nonlinear optics, quantum optics, Rydberg atoms, electromagnetically induced transparency.

## 1. INTRODUCTION

The experimental demonstration of entanglement has generated a tremendous interest in exploiting quantum mechanical properties to improve the transmission and processing of information, a field known as quantum information science.<sup>1</sup> Three intimately related and particularly enticing research fields have emerged over the last three decades: quantum communication,<sup>2-4</sup> metrology beyond the standard quantum limit<sup>5</sup> and quantum computation.<sup>1</sup> For these applications photons are an ideal quantum particle as they robustly and quickly carry information, and techniques to manipulate and detect light at the single-photon level are well established. Two essential elements still actively pursued in the quest for photonic quantum technologies are the on-demand, deterministic generation of single photons and the realization of strong coherent interactions between photons. These elements can be provided by optical materials exhibiting nonlinearities (for example Kerr-type nonlinearities) at the single photon level. Beyond applications to quantum information science, such interactions would pave the way for the simulation of complex quantum systems with light and the creation of strongly correlated states of photons, akin to those observed in cold atomic gases loaded into optical lattices.<sup>6</sup> This possibility has been extensively studied in recent years<sup>7</sup> but many-body quantum photonic states have not been observed yet. Other exotic states of light predicted in highly nonlinear Kerr media include photonics bound states<sup>8,9</sup> and quantum solitons.<sup>10</sup>

Unfortunately optical nonlinearities in traditional media are negligibly weak at intensities corresponding to a single photon pulse. To this day, the most promising approaches to strong photon-photon interactions are cavity Quantum Electro-Dynamics (QED) and Electromagnetically Induced Transparency (EIT). In cavity QED, photons are strongly coupled to a common atom or atomic ensemble by way of a high-finesse optical cavity. The resulting nonlinear photon blockade<sup>11</sup> has been achieved in various systems, for example atoms evanescently coupled to microtoroidal cavities,<sup>12</sup> quantum dots coupled to photonic crystals,<sup>13,14</sup> and superconducting qubits in transmission line resonators.<sup>15</sup> Another spectacular achievement of cavity QED is the realization of conditional phase shifts and coherent quantum gates.<sup>16-18</sup> In EIT, quantum interferences are harnessed to coherently map photons onto large atomic ensembles, giving rise to partially atomic and partially photonic quasi-particles, called polaritons. The purpose of the work presented here is the creation of EIT-based strong polariton-polariton interactions, leading to single-pass optical media with large nonlinear susceptibilities at the single-photon level. This approach simplifies some of the scalability concerns associated with high finesse resonators and opens the door to mesoscopic systems of interacting particles of light.

---

For additional information, e-mail: peyronel@physics.harvard.edu

## 2. RYDBERG EIT: A GIANT OPTICAL KERR EFFECT.

In dielectric media, optical nonlinearities<sup>19</sup> arise when the polarization density is not strictly proportional to the electric field. The third-order susceptibility  $\chi^{(3)}$  is the lowest order nonlinear correction to the polarization of atomic gases, which are centro-symmetric. Third order nonlinearities give rise to the rich physics of four-photon processes, most notably third harmonic generation. In the context of this work, we are interested in the optical Kerr effect, a degenerate case of four-wave mixing where the index of refraction of the medium depends on the intensity of the probe beam (or on that of a second beam for the so-called cross-Kerr effect).

It is possible to estimate the nonlinear response of conventional materials by using the Lorentz model of an elastically bound electron.<sup>19</sup> This simple approach underlines a crucial limitation for most nonlinear media: the third-order nonlinear susceptibility is simultaneously resonant with the linear susceptibility and typically the optical response is strongly dominated by linear effects. To avoid absorption, it is necessary to operate at large detuning from the atomic resonances, which results in a large suppression of the nonlinear susceptibility. In their transparency domain, most conventional materials such as glass, crystals, liquids, gases have a third-order nonlinear susceptibility<sup>19</sup> ranging from  $10^{-22} \text{ V}^{-2} \text{ m}^2$  to  $10^{-19} \text{ V}^{-2} \text{ m}^2$ . Specific nano-particles and polymers reach third-order nonlinear susceptibility up to  $10^{-16} \text{ V}^{-2} \text{ m}^2$ . For reasonable beam sizes and pulse durations, the nonlinear effects are negligible at the single photon level.

In media with narrow optical resonances, typically cold atomic gases, the level structure can be exploited to optimize multi-photon resonances and enhance four-wave mixing. Nevertheless, the large detunings necessary to avoid absorption have so far prevented the observation of nonlinear phase-shifts larger than a few tenths of milliradians per photon.<sup>20</sup> Under EIT conditions,<sup>21</sup> on two-photon resonance, a strong control field cancels the linear absorption and phase shift of the medium. One of the most remarkable properties of EIT is the persistence of third order nonlinearities even as the linear susceptibility vanishes.<sup>22-25</sup> Typical quantum nonlinear effects such as conditional absorption and phase-shift are then on the order of the single atom absorption probability  $\eta$  *i.e.* the probability for the atom on which a first photon is coherently mapped to absorb a second photon. This probability is given by the ratio between the atomic cross-section  $\sigma_0 = \frac{3}{2\pi} \lambda^2$  and the transverse confinement of the light with resonant wavelength  $\lambda$  and is generally smaller than unity due to diffraction. To beat this limit, it is necessary to confine light transversally over extended atomic ensembles<sup>26,27</sup> or use stationary light techniques,<sup>28-30</sup> although these methods have not yet reached the quantum regime of nonlinear optics.

Atomic Rydberg states<sup>31</sup> combine the advantages of a long lifetime (typically  $\sim 100 \mu\text{s}$  for the  $100S_{1/2}$  state of  $^{87}\text{Rb}$  including room-temperature blackbody radiation) and a large dipole moment. The large dipole moment results in long range Van der Waals interactions which shift the Rydberg levels by several times the typical atomic linewidths for atoms located at distances as large as  $10 \mu\text{m}$ . This concept leads to the so-called dipole blockade,<sup>32</sup> which prevents simultaneous optical excitation of several atoms located nearby<sup>33-35</sup> by shifting the doubly excited state out of resonance. Due to their long-lived states, Rydberg levels can be used as a metastable state to enable EIT, playing a similar role to that of the second ground state in a traditional  $\Lambda$ -system. Nevertheless, in contrast to  $\Lambda$ -systems, the dipole-dipole interaction strongly affects the conditions of propagation for simultaneous polaritons due to the detuning of the Rydberg levels far out of resonance, effectively canceling the effect of the control field (see Fig. 1,a). As a result, in the low probe intensity limit, the linear susceptibility of the medium cancels due to EIT, whereas at high power, the response of the medium saturates to that of an ensemble of 2-level atoms with possibly large absorption (for a resonant probe field) or phase-shift (when the field is detuned from the corresponding resonance by a few linewidths).

The nonlinear susceptibility of the medium in the low atomic density limit can be derived by a mean-field approach<sup>36</sup> and is given by (in the absence of decoherence and for a resonant control field):

$$\frac{k}{2} \text{Im}(\chi^{(3)}) = \frac{\pi}{2} \frac{1}{2l_a} \frac{4}{3} \pi r_b^3 \rho \frac{\Omega_p^2}{\Omega_c^2} \quad (1)$$

as a function of the probe wave vector  $k$ , the probe (respectively control) Rabi frequency  $\Omega_p$  (respectively  $\Omega_c$ ), the atomic density  $\rho$ , the absorption length  $l_a = (\rho\sigma_0)^{-1}$  and the blockade radius  $r_b = (2|C_6|\Gamma/\Omega_c^2)^{\frac{1}{6}}$ , *i.e.* the distance  $r$  at which the dipole-dipole induced energy shifts  $\hbar C_6/r^6$  equals half the EIT linewidth  $\gamma_{EIT} = \Omega_c^2/\Gamma$  where  $\Gamma$  is the lifetime of the intermediate excited state. To within a factor of order unity, the nonlinear

susceptibility is the product of the 2-level system linear response  $\chi^{(1)} = i(kl_a)^{-1}$ , the average number of atoms per blockade volume  $N_B = \frac{4}{3}\pi r_b^3 \rho$  and the fraction of the atomic population in the Rydberg state  $\Omega_p^2/\Omega_s^2$ . As a consequence, Rydberg EIT provides dissipative nonlinearities which can be made arbitrarily large by increasing the atomic density. To evaluate the strength of the nonlinearity at the single-photon level, we can use bandwidth-limited pulses<sup>21</sup> of duration  $\tau_p \sim \sqrt{OD} \gamma_{EIT}^{-1}$  (where  $OD = \int dz (l_a(z))^{-1}$  is the total optical depth of the medium) for which the nonlinear effects are on the order of  $N_b \eta$ . The medium can be described in terms of super-atoms<sup>37</sup> with a giant cross-section  $N_b \sigma_0$ , constituted of the  $N_b$  atoms comprised in a single Rydberg blockade volume.

The nonlinearities become dispersive when the probe and control field frequencies are largely detuned by an amount  $\Delta$  from the intermediate state while still satisfying the two-photon resonance condition. In that case, the third-order susceptibility of the medium becomes:

$$\frac{k}{2}\chi^{(3)} = \frac{\pi}{2} \frac{1}{2l_a} \left( \frac{\Gamma}{\Delta} + i \frac{\Gamma^2}{4\Delta^2} \right) \frac{4}{3} \pi r_B^3 \rho \frac{\Omega_p^2}{\Omega_c^2} \quad (2)$$

where the off-resonant blockade radius<sup>38</sup> is  $r_B = (4|C_6\Delta|/\Omega_c^2)^{\frac{1}{6}}$ . The idealized response of the medium in the large blockade fraction regime ( $N_B \Omega_p^2/\Omega_c^2 \sim 1$ ) is that of an ensemble of two-level atoms with absorption  $\sim OD \Gamma^2/\Delta^2$  and phase-shift  $\sim OD \Gamma/\Delta$ , enabling non-dissipative interactions at large detunings  $\Delta \gg \Gamma$ .

In recent years, pioneering experiments have demonstrated this highly nonlinear behavior for cold ensembles in a magneto-optical traps.<sup>39-41</sup> At higher atomic densities, this mean-field approach is not valid as the strong nonlinear effects introduce strong correlations in the probe field. We now present experiments carried out in a dense trapped atomic cloud, entering the regime of quantum nonlinear optics.

### 3. EXPERIMENTAL SETUP

To observe the photon-photon blockade, several key requirements must be fulfilled. First, to eliminate Doppler broadening, the atoms should be cold so that they move by less than an optical wavelength on the microsecond time scale of the experiment. Second, the atomic cloud should be sufficiently dense such that the blockade condition  $r_b \gtrsim l_a$  is fulfilled. Finally, the system should be one-dimensional, *i.e.* the transverse size of the probe beam should be smaller than the blockade radius in order to prevent polaritons from traveling side by side. We fulfill these conditions by trapping a laser-cooled atomic ensemble of <sup>87</sup>Rb and focusing the probe beam to a Gaussian waist  $w_0 = 4.5 \mu\text{m}$ . Using Rydberg states with principal quantum numbers  $46 \leq n \leq 100$ , we can realize blockade radii  $r_b$  between  $3 \mu\text{m}$  and  $13 \mu\text{m}$ , while for our highest atomic densities of  $\mathcal{N} = 2 \times 10^{12} \text{ cm}^{-3}$ , the attenuation length  $l_a$  is below  $2 \mu\text{m}$ .

The laser-cooled ensemble containing up to  $N = 10^5$  atoms is held in a far-detuned optical dipole trap, formed by two orthogonally polarized beams with waists  $w_t = 50 \mu\text{m}$  intersecting at an angle of  $32^\circ$  (see Fig.1,a). The atoms are optically pumped into the state  $|g\rangle = |5S_{1/2}, F = 2, m_F = 2\rangle$  in the presence of a 3.6 G magnetic field along the quantization axis defined by the propagation direction of the probe and control beams along the long axis of the cloud. The probe beam on the  $|g\rangle \rightarrow |e\rangle = |5P_{3/2}, F = 3, m_F = 3\rangle$  transition and the control beam on the  $|e\rangle \rightarrow |r\rangle = |nS_{1/2}, J = \frac{1}{2}, m_J = \frac{1}{2}\rangle$  transition with waist  $w_c = 12.5 \mu\text{m}$  are oppositely circularly polarized. To avoid inhomogeneous light-shift broadening of the two-photon transition, we turn off or modulate the optical dipole trap when we probe the medium. The resonant optical depth of the cloud can be as large as  $OD = 50$ , with initial radial and axial rms cloud dimensions of  $\sigma_\perp = 10 \mu\text{m}$  and  $\sigma_z = 36 \mu\text{m}$ , respectively. The control light is filtered out from the transmitted light, and the photon-photon correlation function  $g^{(2)}(\tau)$  of the probe beam can be measured by means of two photon counters.

### 4. QUANTUM NONLINEAR OPTICS: DISSIPATIVE REGIME.

Probe transmission spectra are presented in Fig. 2,a for large optical depth  $OD = 40$  and the control laser tuned to the Rydberg state  $|100S_{1/2}\rangle$ . At very low incident photon rate  $R_i \leq 1\mu\text{s}^{-1}$ , the spectrum displays an EIT window with 60% transmission. The extraordinary nonlinearity of the Rydberg EIT medium<sup>39</sup> becomes apparent as the incident photon rate is increased: the probe beam is strongly attenuated already at a photon flux of  $R_i \sim 4\mu\text{s}^{-1}$ . To demonstrate that we are operating in a quantum nonlinear regime, we show in Fig. 2,b

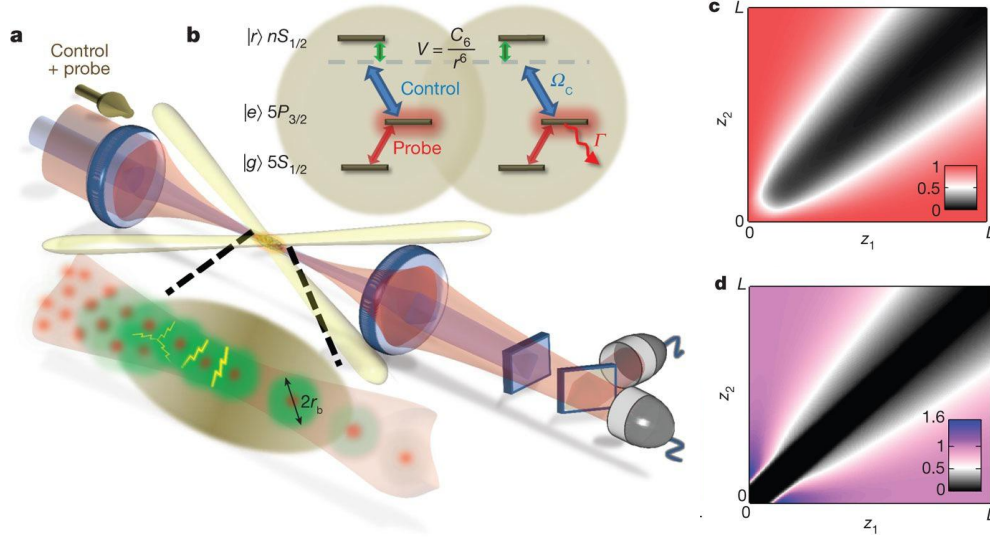


Figure 1. **Interaction between slow photons mediated by Rydberg blockade.** **a, b,** An elongated ensemble of laser-cooled rubidium atoms is prepared in a crossed optical-dipole trap. The control and probe fields couple the ground-state  $|g\rangle$  to a high-lying Rydberg state  $|r\rangle$  via a short-lived excited state  $|e\rangle$ . Under EIT conditions, the probe photons slowly propagate in the medium as Rydberg polaritons. The Rydberg-Rydberg atom interaction  $V(r) = C_6/r^6$  shifts the Rydberg levels out of resonance and blocks simultaneous Rydberg excitation if the interaction exceeds half the EIT-associated linewidth  $\gamma_{\text{EIT}}/2$ . As a result, two Rydberg polaritons cannot both propagate when they are closer than the blockade radius  $r_b = (2C_6/\gamma_{\text{EIT}})^{1/6}$ , set by  $V(r_b) = \gamma_{\text{EIT}}/2$ . **c, d,** Numerical simulations showing the spatial evolution of the probability distribution associated with two photons **(a)** and two Rydberg excitations **(b)** at positions  $(z_1, z_2)$  inside the medium, normalized by their values in the absence of blockade. Two Rydberg excitations are excluded from the blocked range, resulting in the formation of an anti-bunching feature in the light field whose width increases during the propagation due to the finite EIT transmission bandwidth.

the correlation function  $g^{(2)}(\tau)$  of the transmitted probe light, measured at  $R_i = 1.2 \mu\text{s}^{-1}$ . For the most strongly interacting state  $|100S_{1/2}\rangle$  with  $r_b = 13 \mu\text{m} \approx 5l_a \approx 2.9w_0$  we observe strong antibunching with  $g^{(2)}(0) = 0.13(2)$ , largely limited by spurious detection events (dark counts from the detector, imperfect polarization of probe light, residual control light). Subtraction of the independently measured background coincidence counts yields a corrected  $g_c^{(2)}(0) = 0.04(2)$ . These observations are in stark contrast to EIT transmission via a weakly interacting Rydberg state  $|46S_{1/2}\rangle$  with  $r_b = 3 \mu\text{m}$ , where the photon statistics of the transmitted light are similar to those of the incident coherent state (see inset). The  $g^{(2)}$  function also exhibits a local super-Poissonian feature on a range of  $\sim 20 \mu\text{s}$  which we attribute to the occasional population of metastable Rydberg levels not resonantly coupled by the control field to a fast decaying state, inducing classical fluctuations of the transmission.

An important feature of the photon-photon blockade is the correlation time, *i.e.* the width  $\tau_c$  of the anti-bunching feature in  $g^{(2)}(\tau)$ . Interestingly, for  $|100S_{1/2}\rangle$  the photons are anti-bunched over a length scale that exceeds the blockade radius (see top axis of Fig. 2,b), indicating the influence of additional propagation effects beyond the simple picture outlined above. The dependence of  $\tau_c$  on the optical depth, obtained by repeating the measurements for various densities, reveals that the correlation time is of the same order and scales proportionally with the inverse bandwidth of the EIT transparency window  $\gamma_{\text{EIT}}/\sqrt{OD}$ .

To gain insight into these observations, we theoretically analyze the photon propagation dynamics in the weak-probe limit where the average number of photons inside the medium is much less than one. In this case, it suffices to consider two polaritons. The corresponding field component can be described<sup>38</sup> by the two-photon wavefunction  $|\psi_2(t)\rangle = \frac{1}{2} \int dz_1 dz_2 EE(z_1, z_2, t) \hat{\mathcal{E}}^\dagger(z_1) \hat{\mathcal{E}}^\dagger(z_2) |0\rangle$ , where  $\hat{\mathcal{E}}(r)$  denotes the photon field operator and  $|EE(z_1, z_2, t)|^2$  is the probability of finding two photons at locations  $z_1, z_2$ , which relates to the temporal correlation function via  $g^{(2)}(\tau) = |EE(z_1 = L, z_2 = L - v_g\tau)|^2$ . In the absence of decoherence and for a unidimensional system, the steady-state two-photon wavefunction in the medium obeys (see reference<sup>42</sup> for

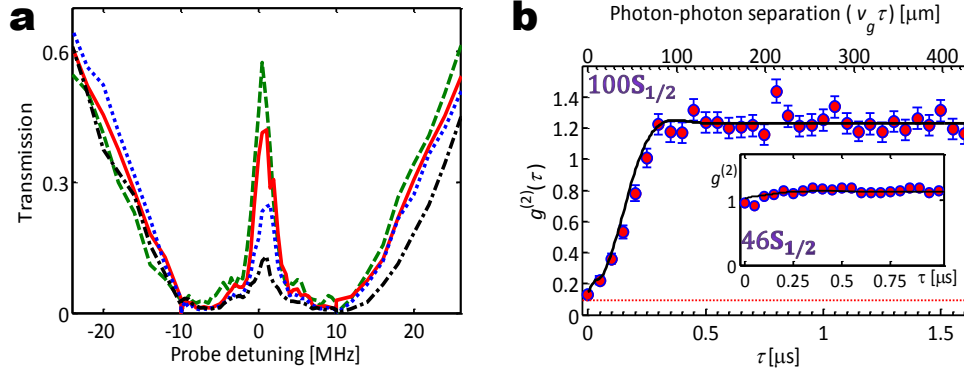


Figure 2. **Rydberg EIT nonlinearities.** **a**, Transmission spectra versus probe detuning at various incoming photon rates:  $R_i = 1\mu\text{s}^{-1}, 2\mu\text{s}^{-1}, 4\mu\text{s}^{-1}, 6\mu\text{s}^{-1}$  (dashed green, solid red, dotted blue, and dot-dashed black, respectively) for  $|100S_{1/2}\rangle$ , optical depth  $OD = 40$ , and pulse delay time  $\tau_d = 340$  ns. The system is nonlinear at a power as low as 0.25 pW. **b**, Photon-photon correlation function  $g^{(2)}(\tau)$  at EIT resonance for the same parameters as in **a** with  $R_i = 1.2\mu\text{s}^{-1}$ . The top axis shows the separation  $v_g\tau$  of polaritons with  $v_g \approx 200$  m/s. The error bars indicate  $1\sigma$  statistical uncertainty. Spurious detection events set a lower bound on  $g^{(2)}$  of 0.09(3) (red dotted line). Inset shows  $g^{(2)}(\tau)$  for the state  $|46S_{1/2}\rangle$  with similar parameters. The solid lines are numerical simulations of the full set of propagation equations including decoherence (see <sup>42</sup> for details).

details):

$$\partial_R EE(z_1, z_2) = -\frac{\mathcal{V}(r)}{l_a} EE(z_1, z_2) + 4l_a \left[ 1 + \mathcal{V}(r) \frac{\Omega_c^2}{\Gamma^2} \right] \partial_r^2 EE(z_1, z_2), \quad (3)$$

where  $R = (z_1 + z_2)/2$ ,  $r = z_1 - z_2$  are the center-of-mass and relative coordinates of the two photons, respectively. The function  $\mathcal{V}(r) = r_b^6 / (r_b^6 - 2ir^6)$  can be regarded as an effective potential that describes the impact of Rydberg-Rydberg interactions.<sup>38</sup> According to equation (3), photon correlations emerge from a combination of two processes as visualized in Fig. 1,c and d: the first term acts inside the blockade radius  $r_b$  and describes absorption with a coefficient  $l_a^{-1}$  as the interaction  $\mathcal{V}$  tunes EIT out of resonance. This would create a sharp dip in the two-photon correlation function with a corresponding correlation time  $\tau_b = r_b/v_g$ . However, if the corresponding spectral width  $\sim \tau_b^{-1}$  is too large, the second diffusion-like term acts to broaden the absorption dip to a width determined by the EIT bandwidth, in agreement with experimental results. To maintain strong two-photon suppression in the presence of diffusion, the loss term must exceed the diffusion on the length scale of the blockade radius, requiring  $r_b > l_a$ .

## 5. QUANTUM NONLINEAR OPTICS: DISPERSIVE REGIME.

We now turn to the dispersive regime, where the photons coherently interact by imprinting on each other a mutual phase-shift. The transition from the dispersive to dissipative regime is obtained by introducing an intermediate detuning  $\Delta$  of the control field from the short-lived intermediate state of the EIT level scheme (see Fig. 3). By operating away from the intermediate atomic resonance, the absorption is reduced and only weakly nonlinear, yielding a purely dispersive nonlinear medium. In this regime, the Rydberg blockade primarily impacts the real part of the linear susceptibility of the medium,<sup>38,40</sup> resulting in a nonlinear phase shift visible in Fig. 3 where a probe photon rate of  $R_i = 5\mu\text{s}^{-1}$  already modifies the medium yielding a probe spectrum close to the bare two-level response. Qualitatively, a substantial two-photon phase shift arises for  $\frac{r_B}{l_a} \frac{\Gamma}{|\Delta|} \gtrsim 1$ . For our parameters using the Rydberg state  $100S_{1/2}$  and  $\Omega_c = 10$  MHz, we have  $r_B \cong 18\mu\text{m}$  at detunings of a few  $\Gamma$ ,  $l_a = 4\mu\text{m}$  at the peak density, and  $w_0 = 4.5\mu\text{m}$ , fulfilling the conditions for strong interactions for  $|\Delta| \lesssim 5\Gamma$ .

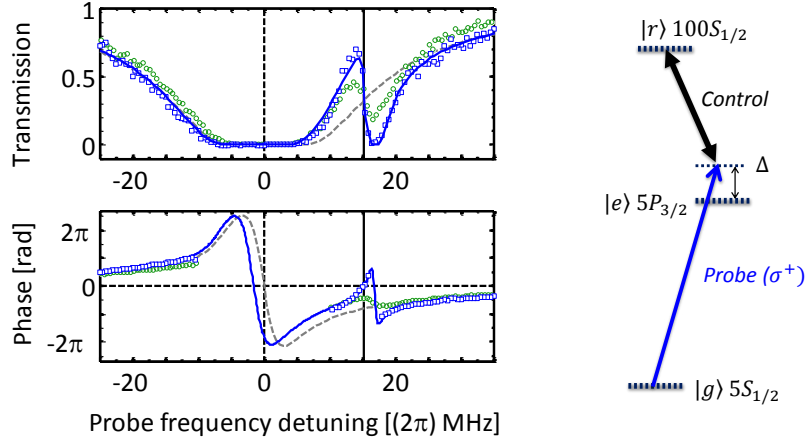


Figure 3. **Rydberg EIT in the dispersive regime.** A weak laser beam near the transition  $|g\rangle \rightarrow |e\rangle$  at 780 nm is sent into a cold rubidium gas driven by a control laser near the transition  $|e\rangle \rightarrow |r\rangle$  at 479 nm. Transmission spectra (top) and phase shift (bottom) for the probe photons with incoming rate of  $R_i = 0.5 \mu s^{-1}$  (blue squares) and  $R_i = 5 \mu s^{-1}$  (green circles), for a control field red-detuned by  $\Delta = 15$  MHz (solid blue line is theory). The spectrum at high probe rate approaches that of the undriven two-level system, which is the idealized limit of a blocked cloud (dashed grey). The solid vertical line corresponds to the EIT resonance.

### 5.1 Conditional phase-shift.

The phase of the  $\sigma^+$ -polarized probe field presented in Fig. 3 is measured by interference with photons which interact only weakly with the atomic medium. More precisely, we prepare input photons in a linearly polarized state  $|V\rangle = (|\sigma^+\rangle + |\sigma^-\rangle)/\sqrt{2}$ , where the  $\sigma^-$  component interacts only negligibly with the medium and serves as a phase reference.

For a dense enough medium, the Rydberg blockade in the dispersive regime induces large conditional phase-shifts.<sup>16</sup> In order to explore these quantum dynamics, we perform a conditional polarization measurement dependent on the time interval between detection events. It consists in measuring the two-photon correlation functions  $g_{\alpha\beta}^{(2)}$  of the transmitted light in different basis  $\alpha, \beta$ . To clarify our approach, we first assume that the system is free of decoherence. In that case, the outgoing one-photon state, detected at time  $t$ , is a pure state:

$$|1\rangle_t = (\eta_+|\sigma^+\rangle_t + \eta_-|\sigma^-\rangle_t)/\sqrt{2}. \quad (4)$$

Here,  $\eta_+$  and  $\eta_-$  characterize the linear susceptibility of the medium, accounting for absorption and phase shift leading to polarization rotation. For two photons arriving at times  $t_1$  and  $t_2$  on two single-photon detectors, the corresponding (unnormalized) outgoing state is:

$$|1, 1\rangle_{t_1, t_2} = \frac{1}{2}[\eta_+^2 \psi(t_1, t_2)|\sigma^+\sigma^+\rangle_{t_1, t_2} + \eta_+\eta_- \chi(t_1, t_2) (|\sigma^+\sigma^-\rangle_{t_1, t_2} + |\sigma^-\sigma^+\rangle_{t_1, t_2}) + \eta_-^2 \mu(t_1, t_2)|\sigma^-\sigma^-\rangle_{t_1, t_2}]. \quad (5)$$

The photon-photon interactions are described by  $\psi(t_1, t_2)$ ,  $\chi(t_1, t_2)$ , and  $\mu(t_1, t_2)$ , which are chosen to be unity in the absence of nonlinear response. Here, the main quantity of interest characterizing the  $\sigma^+$ -photons interaction are the phase and amplitude of the two-photon temporal wavefunction  $\psi(t_1, t_2)$ . The squared amplitude of  $\psi_{t_1, t_2}$  is equal to the normalized second-order correlation function of  $\sigma^+$  photons:

$$|\psi(t_1, t_2)|^2 = g_{++}^{(2)}(t_1, t_2) \quad (6)$$

After independent measurements of the linear transmission  $\eta_+$  and the amplitude of  $\psi$ , the phase  $\arg(\psi_{t_1, t_2})$  can be extracted by additional measurements of the two-photon correlation functions in different polarization bases.

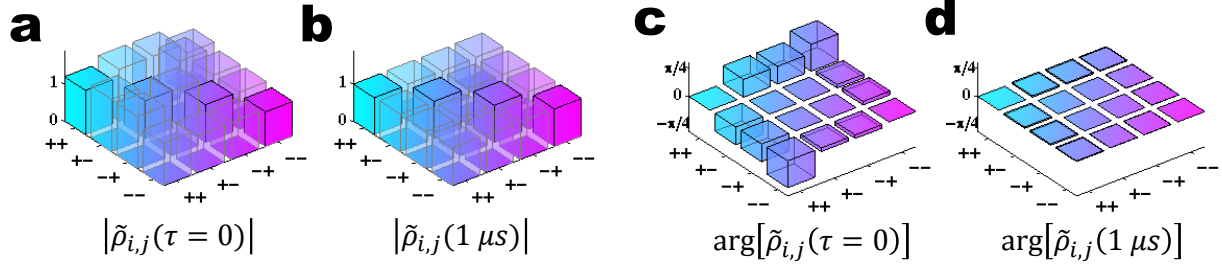


Figure 4. **Tomographic reconstruction of the scaled density matrix  $\tilde{\rho}$ .** Amplitude (a,b) and phase (c,d) of the scaled two-photon density matrix  $\tilde{\rho}_{i,j}(\tau) = \rho_{i,j}(\tau)/[\rho^{(1)} \otimes \rho^{(1)}]_{i,j}$  for two photons with time separation  $\tau = 0$  (a,c) and  $\tau = 1 \mu\text{s}$  (b,d) at a detuning of  $\Delta = 2.3\Gamma$ . All  $\tilde{\rho}_{i,j}(1 \mu\text{s}) = 1$ , as expected in the absence of nonlinearity. The bunching is evident by  $\tilde{\rho}_{+,+,+} > 1$  (a), while the nonlinear (conditional) phase shift is given by  $\arg[\tilde{\rho}_{+,-}] \approx -\pi/4$  (b).

In the presence of decoherence, the outgoing state of the photons must be described by density matrices, with  $\rho^{(1)}(t)$  replacing  $|1\rangle_t\langle 1|_t$ , and  $\rho(t_1, t_2)$  replacing  $|1, 1\rangle_{t_1, t_2}\langle 1, 1|_{t_1, t_2}$ . It is convenient to define the scaled matrix

$$\tilde{\rho}_{i,j}(t_1, t_2) = \frac{\rho_{i,j}(t_1, t_2)}{[\rho^{(1)}(t_1) \otimes \rho^{(1)}(t_2)]_{i,j}} \quad (7)$$

in the basis  $\{|\sigma_1^+\sigma_2^+\rangle, |\sigma_1^+\sigma_2^-\rangle, |\sigma_1^-\sigma_2^+\rangle, |\sigma_1^-\sigma_2^-\rangle\}$ . By definition, all elements of  $\tilde{\rho}$  are equal to 1 in the absence of nonlinearity. For a pure state,  $\arg[\tilde{\rho}_{+,+,-}(t_1, t_2)] = \arg(\psi_{t_1, t_2} \mu_{t_1, t_2}^*)$  is the nonlinear phase-shift of a  $\sigma^+\sigma^+$  photon-pair with respect to that of the weakly interacting  $\sigma^-\sigma^-$  pair.

The resulting scaled density matrices are plotted in Fig. 4 in the limits of proximal ( $t_1 = t_2$ ) and distant (non-interacting)  $|t_1 - t_2| = 1 \mu\text{s}$  photons. As expected, at large time separation, the elements of the scaled matrix are all equal to unity. For photons exiting the medium simultaneously, we observe the existence of a large conditional phase-shift between  $|\sigma^+\sigma^+\rangle$  and  $|\sigma^-\sigma^-\rangle$ . The small phase emerging between the  $|\sigma^+\sigma^-\rangle$  and  $|\sigma^-\sigma^+\rangle$  components underlines that photons with opposite polarizations interact very weakly.

The probability density of two interacting  $\sigma^+$  photons,  $g_{++}^{(2)}(t_1, t_2)$ , and the nonlinear phase, acquired by the  $\sigma^+\sigma^+$  pair relative to a non-interacting  $\sigma^-\sigma^-$  pair,  $\phi = \arg[\tilde{\rho}_{+,+,-}]$ , are shown in Figs. 5,a and b for  $\Delta = 14 \text{ MHz}$ . Clearly visible is the bunching of photons, *i.e.* an increased probability for photons to exit the medium simultaneously ( $t_1 \approx t_2$ ), and a substantial nonlinear two-photon phase shift of  $-0.5 \text{ rad}$  in that region. Here  $t_1$  and  $t_2$  belong to the central region of the  $5 \mu\text{s}$  pulse, where the experiments is steady state. In that regime, the correlation function only depends on the detection time difference  $\tau = t_2 - t_1$  and can be averaged along the diagonal lines. Figure 5,c shows the intensity correlation in the dissipation-dominated antibunching regime at  $\Delta = 0$  and in the dispersive regime at  $|\Delta| > \Gamma$  and Fig. 5,d displays the nonlinear phase for two different detunings. The central result of this work is the large nonlinear Kerr phase-shift  $> \pi/4$  at the single photon level for a medium with a large linear transmission of order 50%. The linear transmission is technically limited by the ground- to Rydberg- state decoherence, which arises from the probe and control field linewidth and the finite temperature of the atoms. This record conditional phase-shift outside the context of cavity QED is accompanied by the emergence of a visible bunching feature in the probability density of the two-photon wavefunction.

The transition from the dissipative to the dispersive regime with increasing  $|\Delta|$  is summarized in Figs. 6,a,b. In the dispersive regime, the nonlinear phase shift  $\phi(\tau = 0)$  can reach  $(-0.32 \pm 0.02)\pi$ , at a detuning  $\Delta = 9 \text{ MHz}$ . As expected from the refractive index discrepancy between the 2-level and 3-level atomic ensemble, the blockade generates a large condition phase shift at  $|\Delta| \gtrsim \Gamma$ , which is ultimately limited by the absorption length  $l_a$  of the medium and the total optical depth  $OD$ . The absolute value of the nonlinear phase  $|\phi|$  exhibits asymmetries under a sign change of the detuning  $\Delta$  from the intermediate atomic  $|e\rangle$  state. In particular, at negative values of  $\Delta$ , corresponding to a blue-detuning of the control field, the phase-shift is strongly reduced and deviates

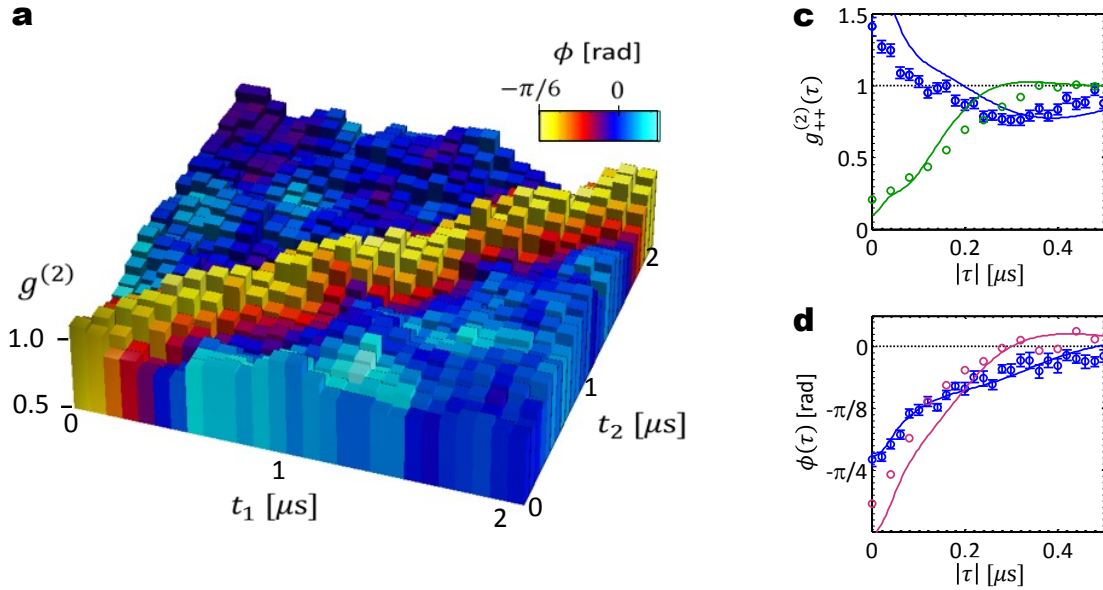


Figure 5. **Conditional phase-shift and photon bunching.** **a**, Measured second-order correlation function (bar height) and nonlinear phase shift (color scale) of interacting photon pairs at  $\Delta = 2.3\Gamma$ . The photons are detected at times  $t_1$  and  $t_2$ . **b**, Second-order correlation function displayed as a function of the time difference  $|\tau| = |t_1 - t_2|$  between the photons, showing the transition from anti-bunching on resonance ( $\Delta = 0$ , green) to bunching at large detuning ( $\Delta = 2.3\Gamma$ , blue). Points are experimental data, lines are full numerical simulations. **c**, Nonlinear phase-shift versus  $|\tau|$  for two different detunings ( $\Delta = 1.5\Gamma$ , purple, and  $\Delta = 2.3\Gamma$ , blue). The  $1\sigma$  error is  $\pm 30$  mrad, dominated by photon shot noise.

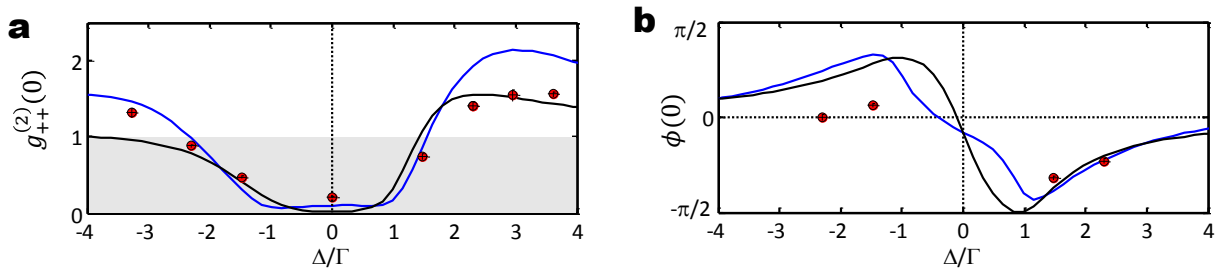


Figure 6. **Transition between the dissipative and dispersive regimes.** Equal-time two-photon correlation  $g_{++}^{(2)}(0)$  (**a**) and nonlinear phase  $\phi(0)$  (**b**) versus detuning  $\Delta$  from the intermediate state  $|e\rangle$ . Blue lines are full theoretical simulations, while black lines are the result of the Schrodinger-equation approximation, assuming a simplified delta-function potential. Vertical error bars represent  $1\sigma$  and horizontal error bars are  $\pm 0.5$  MHz.

from the predicted results given by our full theoretical simulations. In principle, the symmetry between positive and negative  $\Delta$  is broken by the repulsive dipole interaction of the  $100S_{1/2}$  states. For negative  $\Delta$ , a positive energy shift of the Rydberg level of order  $\Omega^2/|\Delta|$  tunes the two-photon Raman absorption dip in resonance with the probe field satisfying the two-photon resonance condition for unperturbed levels. On the contrary, for  $\Delta > 0$ , positive energy shifts of the Rydberg level detunes the two-photon absorption dip further away from the two-photon resonance. For negative  $\Delta$ , this asymmetry introduces a dissipative interaction between photons at a distance equating the Van der Waals interaction and the control field Stark-shift, which is absent from the regime  $\Delta > 0$ .

## 5.2 Two-photon bound state.

We now turn to the explanation of the bunching feature, depicted in Figs. 5,c, 6,a. The propagation of  $\sigma^+$ -polarized photon pairs in the medium can be understood by first considering an idealized situation with no decoherence between the Rydberg state and the ground state. Then the steady-state in a one-dimensional homogenous medium can be described by a two-photon wavefunction  $\psi(z_1, z_2)$ , whose evolution is approximately governed by a simple equation (see <sup>43</sup> for details) in the center-of-mass  $R = (z_1 + z_2)/2$  and relative  $r = z_1 - z_2$  coordinates:

$$i\partial_R\psi = 4l_a \left[ i + \frac{2\Delta}{\Gamma} - \mathcal{V}(r) \frac{\Omega_c^2}{\Gamma^2} \right] \partial_r^2\psi + \frac{\mathcal{V}(r)}{l_a}\psi. \quad (8)$$

Here the effective potential:

$$\mathcal{V}(r) = \left[ i + 2\frac{\Delta}{\Gamma} (1 + 2r^6/r_B^6) \right]^{-1} \quad (9)$$

approaches  $(i + 2\Delta/\Gamma)^{-1}$  inside the blockaded volume ( $|r| < r_B$ ), and zero outside. To a good approximation valid at small  $|\tau|$ , the solution relates to the temporal wavefunction  $\psi(\tau)$  defined in the previous section and to our measurements in time domain via:

$$\psi(R = L, r = v_g\tau) \sim \psi(\tau) = \sqrt{g_{++}^{(2)}(\tau)} e^{i\phi(\tau)} \quad (10)$$

Far off resonance ( $|\Delta| \gg \Gamma, \Omega_c$ ), Eq. 8 corresponds to a Schroedinger equation with the center-of-mass propagation distance  $R$  playing the role of effective time. The photons' effective mass  $m \propto -\Gamma/(16l_a\Delta)$  can be positive or negative depending on the sign of the detuning  $\Delta$ . The sign of the potential also changes with  $\Delta$  and the potential is a well for  $\Delta < 0$  and a barrier for  $\Delta > 0$ . Nevertheless, because the boundary condition  $\psi(R = 0, r) = 1$  is unchanged under complex conjugation  $\psi \rightarrow \psi^*$ , the dynamics for positive  $\Delta$  also correspond to a particle with positive mass in a potential well, as immediately derived by taking the complex conjugate of the Schroedinger equation, leading to an effective attractive force in both cases and opposite nonlinear phase-shifts. As mentioned earlier, the potential for  $\Delta < 0$  also exhibits additional features near the edges of the well, corresponding to a Raman resonance  $|g\rangle \rightarrow |r\rangle$  for the interaction-shifted Rydberg state at some interatomic distance near  $|r| = r_B$  and these features are likely responsible for the deviation from (anti-)symmetry under the change of the sign of  $\Delta$  displayed in Fig. 6.

In the experimentally relevant regime, the effective potential supports only one bound-state  $\psi_B(r)$  depicted in Fig. 7,a. The initial wavefunction  $\psi(R = 0, r) = 1$  is a superposition of  $\psi_B(r)$  and the continuum of scattering states. The accumulation of probability near  $r = 0$  can then be understood as arising from the interference between the bound and scattering states that evolve at different frequencies. The exact evolution of the real and complex parts of the bound- and scattering states under Eq.8 is plotted in Figs. 7c,d. As shown in Fig. 7a, where the temporal wavefunction  $\psi(\tau)$  has been rescaled by the group velocity, the observed bunching feature in  $g_{++}^{(2)}$  reflects the wavefunction of the two-photon bound state. The size of the two-photon bound state and correspondingly the width of the bunching feature  $2\tau_b v_g \sim 70 \mu\text{m}$ , exceed the width of the potential well of  $2r_B \sim 35 \mu\text{m}$ , as expected for a potential with one weakly bound state. As a consequence, the potential is well approximated by a simple  $\delta$ -potential. Fig. 6 displays the solution of the Schroedinger-like equation 3 with a simplified delta-function potential (black curves), which agree well with our measurements and the theoretical predictions and capture the essential features of the nonlinear two-photon propagation.

## 5.3 Dependence on two-photon detuning.

Additional experimental evidence for the bound-state dynamics is obtained by tuning the probe field relative to the EIT resonance, thereby varying the strength of the two-photon interaction potential. As the probe detuning approaches the Raman resonance,  $\delta \sim \Omega_c^2/(4\Delta)$ , the difference in refractive indices inside and outside the blockade radius increases and the potential deepens (see Fig. 3). Consequently, the bound state becomes more localized and the bunching, quantified by  $g_{++}^{(2)}(0)$ , is enhanced, as evidenced in Fig. 8,a and b. In that regime, the measured correlation function differs significantly from the prediction from our full theoretical model. At Raman resonance, the nonlinear interactions become mainly dissipative: single photons are strongly absorbed

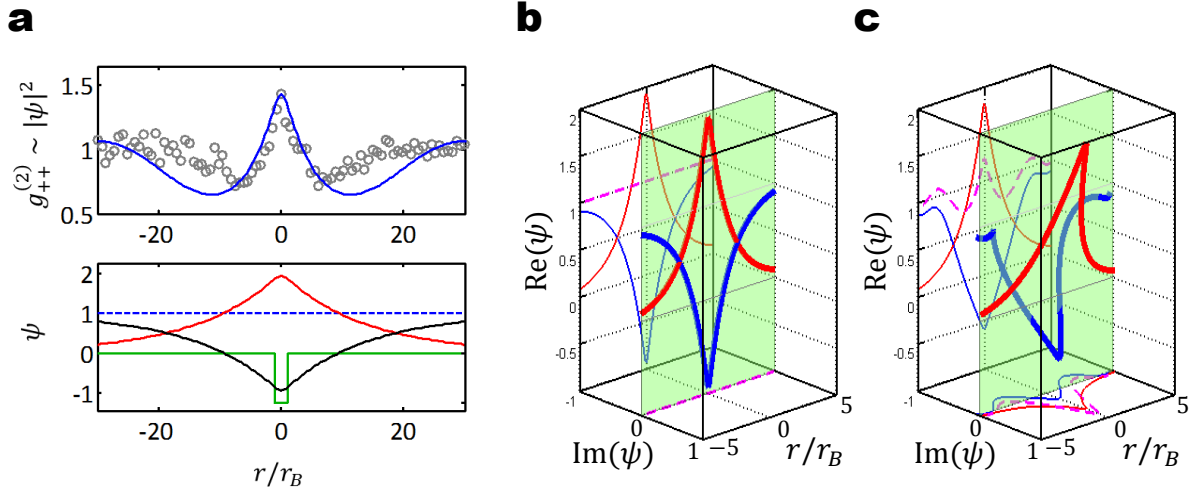


**Figure 7. Two-photon bound state evolution.** **a**, Photon bunching and two-photon bound state. Theoretically predicted photon-photon correlation function in the Schrodinger-equation approximation (top, blue line) for  $\Delta = 14$  MHz, with a potential well of width  $2r_B$  (bottom, green line). The bound state (bottom, red) and the superposition of scattering states (bottom, black) form the initial wave function  $\psi = 1$  (bottom, dashed blue). The two-photon bound state results in the observed bunching in the correlation function  $g_{++}^{(2)} \sim |\psi|^2$  (top, gray circles), where time has been converted into distance via the group velocity  $v_g$ . The boundary effects resulting from the finite extent of the atom cloud become important for  $|r| \geq 5 r_B$ . **b,c**, Detailed visualization of the solution  $\psi(R, r)$  to the Schrodinger Eq. 8 at the beginning ( $R = 0$ ) and at the end ( $R = L$ ) of the medium for  $\Delta = 2.3\Gamma$  and  $r_B = 0.15L$ .  $\psi$  is a superposition of the unique bound eigenstate of the system (thick red) and a set scattering eigenstates (thick blue). For clearer visualization, the real and imaginary part of the bound (red) and scattering (blue) states, as well as the total wavefunction (dashed purple), are projected on the back and bottom planes of the tri-dimensional drawing. Initially, the bound state and the scattering states interfere to produce the boundary condition  $\psi = 1$ . On the short timescale corresponding to our parameters, the unitary evolution mainly rotates the bound state with respect to the scattering state, giving rise to a bunching peak on the real and imaginary part of  $\psi$ .

by the medium, with an opacity equal to the resonant  $OD$  in the absence of decoherence. Two-photon states are transmitted with large probability as the Rydberg blockade tunes the large absorption dip out of resonance. This strongly modifies the correlation-function: in the denominator, the transmission is dominated by multi-photon states, dark counts and polarization imperfections. The last two-effect strongly reduce the maximum observable correlation function, while the first effect requires the inclusion of higher many-body states in the theoretical model for our typical probe photon incoming rates. The numerator of the correlation function also possibly requires a many-body model to capture our experimental results. As shown in Fig. 8,c, for measurements at very low probe power, same-time intensity correlations  $g_{++}^{(2)}(0)$  as large as 6 are observed.

The opposite regime,  $\Delta > 0, \delta < 0$ , shifts the two-photon transitions towards the maximum of the transmission peak at  $\delta \sim -\frac{\Delta}{\Gamma}\gamma$  where  $\gamma$  is the Rydberg- to ground-state decoherence rate. The potential depth is reduced and the transmission visibly higher than that of the 2-level medium. As shown in Fig. 8d, a clear bunching peak is still visible in the correlation function, followed by a wider sub-poissonian feature. The existence of the bunching feature in a regime where dissipative interactions lead to anti-bunching is a clear signature of the domination of the dispersive interaction for our experimental parameters. For this regime, the theoretical simulations are in good agreement with our experimental results, confirming that the evolution of the two-photon wavepacket is dominated by the attractive force between the photons.

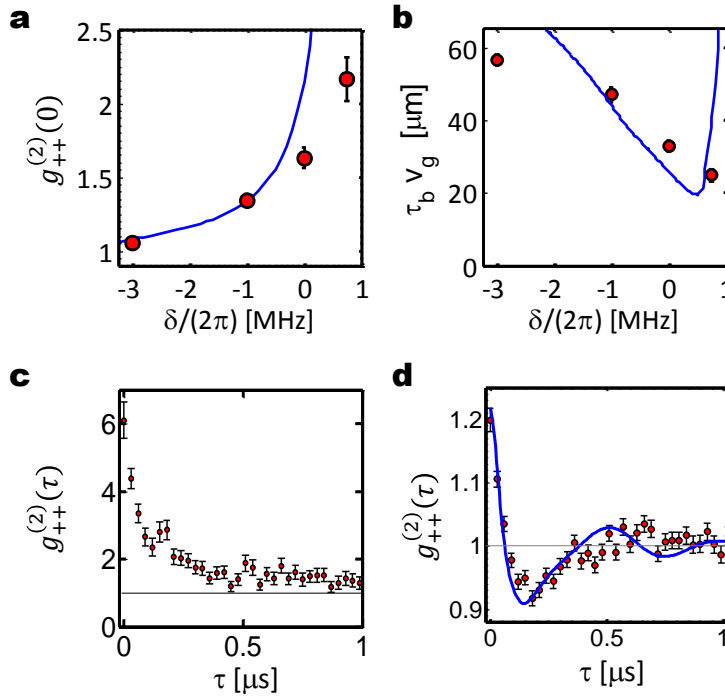


Figure 8. **Effect of the two-photon detuning.** Equal-time correlation function (a) and spatial extent of the bunching feature (b) versus Raman detuning  $\delta$  from the EIT resonance  $|g\rangle \rightarrow |r\rangle$  for  $\Delta = 3\Gamma$ , showing increased photon-photon attraction due to a deeper potential near Raman resonance. The characteristic bunching-timescale  $\tau_b$  is the half-width of the cusp feature of  $g_{++}^{(2)}$ , defined at half-height between the peak value at  $\tau = 0$  and the local minimum closest to  $\tau = 0$ . Error bars correspond to  $\pm 1\sigma$ . The theoretical model (solid line) breaks down close to the Raman resonance at  $\delta = 1.3 \text{ MHz} \approx \Omega_c^2/(4\Delta)$ , where the single-photon component of the probe field is strongly absorbed. **c**, Intensity correlation function for interacting photons  $g_{++}^{(2)}(\tau)$  measured at the two-photon Raman absorption dip, for  $\Delta = 1.5\Gamma$ . The dissipative interactions lead to large bunching effects (the medium is strongly absorptive for single photons and transparent for multi-photon states). The value  $g_{++}^{(2)}(0) \sim 6$  is limited by background noise and transmitted many-photon states, which dominate the average measured rates. **d**, Intensity correlation function for interacting photons  $g_{++}^{(2)}(\tau)$  measured at the peak probe transmission for  $\Delta = 3\Gamma$ . The persistence of the bunching feature in a regime where dissipative interactions result in anti-bunching is a clear signature of strong dispersive effects.

## 6. OUTLOOK.

The realization of coherent, dispersive photon-photon interactions opens up several new research directions. These include the exploration of a novel quantum matter composed from strongly interacting, massive photons.<sup>44</sup> Measurements of higher-order correlation functions may give direct experimental access to quantum solitons composed of a few interacting bosons,<sup>45</sup> or to the detection of crystalline states of a photonic gas.<sup>44</sup> By colliding two counterpropagating photons, it may be possible to imprint a spatially homogeneous phase shift of  $\pi$  on the photon pair, corresponding to a deterministic quantum gate<sup>38</sup> for scalable optical quantum computation.<sup>46</sup> Finally, by accessing other Rydberg states via, *e.g.*, microwave transitions, it may become possible to control the state of multi-photon pulses with just one quantum of light, thereby realizing a single-photon transistor<sup>8</sup> for applications in quantum networks.

## REFERENCES

- [1] Nielsen, M. A. and Chuang, I. L., [*Quantum Computation and Quantum Information*], Cambridge University Press (2000).

- [2] Cirac, J. I., Zoller, P., Kimble, H. J., and Mabuchi, H., “Quantum state transfer and entanglement distribution among distant nodes in a quantum network,” *Phys. Rev. Lett.* **78**, 3221–3224 (1997).
- [3] Duan, L. M., Lukin, M. D., Cirac, J. I., and Zoller, P., “Long-distance quantum communication with atomic ensembles and linear optics,” *Nature* **414**(6862), 413–418 (2001).
- [4] Kimble, H. J., “The quantum internet,” *Nature* **453**(7198), 1023–1030 (2008).
- [5] Giovannetti, V., Lloyd, S., and Maccone, L., “Quantum-enhanced measurements: Beating the standard quantum limit,” *Science* **306**(5700), 1330–1336 (2004).
- [6] Greiner, M., Mandel, O., Esslinger, T., Hansch, T. W., and Bloch, I., “Quantum phase transition from a superfluid to a mott insulator in a gas of ultracold atoms,” *Nature* **415**(6867), 39–44 (2002).
- [7] Carusotto, I. and Ciuti, C., “Quantum fluids of light,” *Rev. Mod. Phys.* **85**, 299–366 (2013).
- [8] Chang, D. E., Sorensen, A. S., Demler, E. A., and Lukin, M. D., “A single-photon transistor using nanoscale surface plasmons,” *Nat Phys* **3**(11), 807–812 (2007).
- [9] Shen, J.-T. and Fan, S., “Strongly correlated two-photon transport in a one-dimensional waveguide coupled to a two-level system,” *Phys. Rev. Lett.* **98**, 153003 (2007).
- [10] Drummond, P. D., Shelby, R. M., Friberg, S. R., and Yamamoto, Y., “Quantum solitons in optical fibres,” *Nature* **365**(6444), 307–313 (1993).
- [11] Birnbaum, K. M., Boca, A., Miller, R., Boozer, A. D., Northup, T. E., and Kimble, H. J., “Photon blockade in an optical cavity with one trapped atom,” *Nature* **436**(7047), 87–90 (2005).
- [12] Dayan, B., Parkins, A. S., Aoki, T., Ostby, E. P., Vahala, K. J., and Kimble, H. J., “A photon turnstile dynamically regulated by one atom,” *Science* **319**(5866), 1062–1065 (2008).
- [13] Faraon, A., Fushman, I., Englund, D., Stoltz, N., Petroff, P., and Vuckovic, J., “Coherent generation of non-classical light on a chip via photon-induced tunnelling and blockade,” *Nat Phys* **4**(11), 859–863 (2008).
- [14] Reinhard, A., Volz, T., Winger, M., Badolato, A., Hennessy, K. J., Hu, E. L., and Imamoglu, A., “Strongly correlated photons on a chip,” *Nat Photon* **6**(2), 93–96 (2012).
- [15] Lang, C., Bozyigit, D., Eichler, C., Steffen, L., Fink, J. M., Abdumalikov, A. A., Baur, M., Filipp, S., da Silva, M. P., Blais, A., and Wallraff, A., “Observation of resonant photon blockade at microwave frequencies using correlation function measurements,” *Phys. Rev. Lett.* **106**, 243601 (2011).
- [16] Turchette, Q. A., Hood, C. J., Lange, W., Mabuchi, H., and Kimble, H. J., “Measurement of conditional phase shifts for quantum logic,” *Phys. Rev. Lett.* **75**, 4710–4713 (1995).
- [17] Fushman, I., Englund, D., Faraon, A., Stoltz, N., Petroff, P., and Vuckovic, J., “Controlled phase shifts with a single quantum dot,” *Science* **320**(5877), 769–772 (2008).
- [18] Kirchmair, G., Vlastakis, B., Leghtas, Z., Nigg, S. E., Paik, H., Ginossar, E., Mirrahimi, M., Frunzio, L., Girvin, S. M., and Schoelkopf, R. J., “Observation of quantum state collapse and revival due to the single-photon kerr effect,” *Nature* **495**(7440), 205–209 (2013).
- [19] Boyd, R. W., [*Nonlinear Optics*], Elsevier (2008).
- [20] Venkataraman, V., Saha, K., and Gaeta, A. L., “Phase modulation at the few-photon level for weak-nonlinearity-based quantum computing,” *Nature Photonics* **7**, 138–141 (2012).
- [21] Fleischhauer, M., Imamoglu, A., and Marangos, J. P., “Electromagnetically induced transparency: Optics in coherent media,” *Rev. Mod. Phys.* **77**, 633–673 (2005).
- [22] Harris, S. E., Field, J. E., and Imamoglu, A., “Nonlinear optical processes using electromagnetically induced transparency,” *Phys. Rev. Lett.* **64**, 1107–1110 (1990).
- [23] Schmidt, H. and Imamoglu, A., “Giant kerr nonlinearities obtained by electromagnetically induced transparency,” *Opt. Lett.* **21**(23), 1936–1938 (1996).
- [24] Harris, S. and Yamamoto, Y., “Photon switching by quantum interference,” *Phys. Rev. Lett.* **81**, 3611 (1998).
- [25] Harris, S. and Hau, L. V., “Nonlinear optics at low light levels,” *Phys. Rev. Lett.* **82**(23), 4611(4) (1998).
- [26] Bajcsy, M., Hofferberth, S., Balic, V., Peyronel, T., Hafezi, M., Zibrov, A. S., Vuletic, V., and Lukin, M. D., “Efficient all-optical switching using slow light within a hollow fiber,” *Phys. Rev. Lett.* **102**, 203902 (2009).
- [27] Dawkins, S. T., Mitsch, R., Reitz, D., Vetsch, E., and Rauschenbeutel, A., “Dispersive optical interface based on nanofiber-trapped atoms,” *Phys. Rev. Lett.* **107**, 243601 (2011).

- [28] Andre, A. and Lukin, M., “Manipulating light pulses via dynamically controlled photonic band gas,” *Phys. Rev. Lett.* **89**, 143602 (2002).
- [29] André, A., Bajcsy, M., Zibrov, A. S., and Lukin, M. D., “Nonlinear optics with stationary pulses of light,” *Phys. Rev. Lett.* **94**, 063902 (2005).
- [30] Chen, Y.-H., Lee, M.-J., Hung, W., Chen, Y.-C., Chen, Y.-F., and Yu, I. A., “Demonstration of the interaction between two stopped light pulses,” *Phys. Rev. Lett.* **108**, 173603 (2012).
- [31] Saffman, M., Walker, T. G., and Mølmer, K., “Quantum information with rydberg atoms,” *Rev. Mod. Phys.* **82**, 2313–2363 (2010).
- [32] Lukin, M. D., Fleischhauer, M., Cote, R., Duan, L. M., Jaksch, D., Cirac, J. I., and Zoller, P., “Dipole blockade and quantum information processing in mesoscopic atomic ensembles,” *Phys. Rev. Lett.* **87**, 037901 (2001).
- [33] Urban, E., Johnson, T. A., Henage, T., Isenhower, L., Yavuz, D. D., Walker, T. G., and Saffman, M., “Observation of rydberg blockade between two atoms,” *Nat Phys* **5**(2), 110–114 (2009).
- [34] Gaetan, A., Miroshnychenko, Y., Wilk, T., Chotia, A., Viteau, M., Comparat, D., Pillet, P., Browaeys, A., and Grangier, P., “Observation of collective excitation of two individual atoms in the rydberg blockade regime,” *Nat Phys* **5**(2), 115–118 (2009).
- [35] Dudin, Y. O. and Kuzmich, A., “Strongly interacting rydberg excitations of a cold atomic gas,” *Science* **336**(6083), 887–889 (2012).
- [36] Sevinçli, S., Henkel, N., Ates, C., and Pohl, T., “Nonlocal nonlinear optics in cold rydberg gases,” *Phys. Rev. Lett.* **107**, 153001 (2011).
- [37] Pritchard, J., Weatherill, K., and Adams, C., “Non-linear optics using cold rydberg atoms,” *arXiv:1205.4890v1* (May 2012).
- [38] Gorshkov, A. V., Otterbach, J., Fleischhauer, M., Pohl, T., and Lukin, M. D., “Photon-photon interactions via rydberg blockade,” *Phys. Rev. Lett.* **107**, 133602 (2011).
- [39] Pritchard, J. D., Maxwell, D., Gauguet, A., Weatherill, K. J., Jones, M. P. A., and Adams, C. S., “Cooperative atom-light interaction in a blockaded rydberg ensemble,” *Phys. Rev. Lett.* **105**, 193603 (Nov 2010).
- [40] Parigi, V., Bimbarb, E., Stanojevic, J., Hilliard, A. J., Nogrette, F., Tualle-Brouri, R., Ourjoumtsev, A., and Grangier, P., “Observation and measurement of interaction-induced dispersive optical nonlinearities in an ensemble of cold rydberg atoms,” *Phys. Rev. Lett.* **109**, 233602 (2012).
- [41] Sevinçli, S., Ates, C., Pohl, T., Schempp, H., Hofmann, C. S., Gunter, G., Amthor, T., Weidemüller, M., Pritchard, J. D., Maxwell, D., Gauguet, A., Weatherill, K. J., Jones, M. P. A., and Adams, C. S., “Quantum interference in interacting three-level rydberg gases: coherent population trapping and electromagnetically induced transparency,” *J. Phys. B: At. Mol. Opt. Phys.* **44**, 184018 (2011).
- [42] Peyronel, T., Firstenberg, O., Liang, Q.-Y., Hofferberth, S., Gorshkov, A. V., Pohl, T., Lukin, M. D., and Vuletic, V., “Quantum nonlinear optics with single photons enabled by strongly interacting atoms,” *Nature* **488**, 57–60 (2012).
- [43] Firstenberg, O., Peyronel, T., Liang, Q.-Y., Gorshkov, A. V., Lukin, M. D., and Vuletic, V., “Quantum nonlinear optics with single photons enabled by strongly interacting atoms,” *Nature* **502**, 71–75 (2013).
- [44] Chang, D. E., Gritsev, V., Morigi, G., Vuletic, V., Lukin, M. D., and Demler, E. A., “Crystallization of strongly interacting photons in a nonlinear optical fibre,” *Nat Phys* **4**(11), 884–889 (2008).
- [45] Drummond, P. D. and He, H., “Optical mesons,” *Phys. Rev. A* **56**, R1107–R1109 (1997).
- [46] Isenhower, L., Urban, E., Zhang, X. L., Gill, A. T., Henage, T., Johnson, T. A., Walker, T. G., and Saffman, M., “Demonstration of a neutral atom controlled-not quantum gate,” *Phys. Rev. Lett.* **104**, 010503 (2010).